# Resonant and non-resonant generation and focusing of surface plasmons with circular gratings

**Jennifer M. Steele[‡\*], Zhaowei Liu[‡], Yuan Wang, and Xiang Zhang**

*5130 Etcheverry Hall, NSF Nanoscale Science and Engineering Center (NSEC), University of California, Berkeley, California, 94720*

[‡]*The first two authors contributed equally to this work*

*\*The present address for Jennifer M. Steele is Department of Physics and Astronomy, Trinity University, San Antonio, Texas 78212*

*xiang@berkeley.edu*

*http://xlab.me.berkeley.edu*

**Abstract:** We report the generation and focusing of surface plasmon polariton (SPP) waves from normally incident light on a planar circular grating milled into a silver film. The focusing mechanism is explained by using a simple coherent interference model of SPP generation on the circular grating by the incident field. Experimental results concur well with theoretical predictions and highlight the requirement for the phase matching of SPP sources in the grating to achieve the maximum enhancement of the SPP wave at the focal point. NSOM measurements show that the plasmonic lens achieves more than a 10-fold intensity enhancement over the intensity of a single ring of the in-plane field components at the focus when the grating design is tuned to the SPP wavelength. We discuss the technique's adaptability for surface enhanced nano-scale spectroscopy.

**References and links:**

1. A. Dahlin, M. Zach, T. Rindzevicius, M. Kall, D. S. Sutherland, and F. Hook, "Localized surface plasmon resonance sensing of lipid-membrane-mediated biorecognition events," J. Am. Chem. Soc. **127**, 5043-5048 (2005).
2. E. Hutter, and J. H. Fendler, "Exploitation of localized surface plasmon resonance," Adv. Mater. **16**, 1685-1706 (2004).
3. S. A. Maier, and H. A. Atwater, "Plasmonics: Localization and guiding of electromagnetic energy in metal/dielectric structures," J. Appl. Phys. **98**, 011101 (2005).
4. A. J. Haes, and R. P. Van Duyne, "A unified view of propagating and localized surface plasmon resonance biosensors," Anal. Bioanal. Chem. **379**, 920-930 (2004).
5. J. B. Jackson, and N. J. Halas, "Surface-enhanced Raman scattering on tunable plasmonic nanoparticle substrates," Proc. Natl. Acad. Sci. USA **101**, 17930-17935 (2004).
6. C. L. Haynes, A. D. McFarland, R. P. Van Duyne, "Surface-enhanced Raman spectroscopy," Anal. Chem. **77**, 338A-346A (2005).
7. A. J. Haes, C. L. Haynes, A. D. McFarland, G. C. Schatz, R. P. Van Duyne, and S. L. Zou, "Plasmonic materials for surface-enhanced sensing and spectroscopy," MRS Bulletin **30**, 368-375 (2005).
8. A. D. McFarland, M. A. Young, J. A. Dieringer, R. P. Van Duyne, "Wavelength-scanned surface-enhanced Raman excitation spectroscopy," J. Phys. Chem. B **109**, 11279-11285 (2005).
9. H. Ditlbacher, J. R. Krenn, G. Schider, A. Leitner, F. R. Aussenegg, "Two-dimensional optics with surface plasmon polaritons," Appl. Phys. Lett. **81**, 762-1764 (2002).
10. A. L. Stepanov, J. R. Krenn, H. Ditlbacher, A. Hohenau, A. Drezet, B. Steinberger, A. Leitner, and F. R. Aussenegg, "Quantitative analysis of surface plasmon interaction with silver nanoparticles," Opt. Lett. **30**, 1524-1526 (2005).

11. H. Ditlbacher, J. R. Krenn, A. Leitner, and F. R. Aussenegg, "Surface plasmon polariton-based optical beam profiler," Opt. Lett. **29**, 1408-1410 (2004).
12. M. Salerno, J. R. Krenn, B. Lamprecht, G. Schider, H. Ditlbacher, N. Felidj, A. Leitner, and F. R. Aussenegg, "Plasmon polaritons in metal nanostructures: the optoelectronic route to nanotechnology," Opto-Electronics Rev. **10**, 217-224 (2002).
13. F. Tam, C. Moran, and N. Halas, "Geometrical parameters controlling sensitivity of nanoshell plasmon resonances to changes in dielectric environment," J. Phys. Chem. B **108**, 17290-17294 (2004).
14. N. Nath, and A. Chilkoti, "Label-free biosensing by surface plasmon resonance of nanoparticles on glass: Optimization of nanoparticle size," Anal. Chem. **76**, 5370-5378 (2004).
15. J. Aizpurua, P. Hanarp, D. S. Sutherland, M. Kall, G. W. Bryant, and F. J. G. de Abajo, "Optical properties of gold nanorings," Phys. Rev. Lett. **90**, 057401 (2003).
16. A. D. McFarland, and R. P. Van Duyne, "Single silver nanoparticles as real-time optical sensors with zeptomole sensitivity," Nano. Lett. **3**, 1057-1062 (2003).
17. Z. W. Liu, J. M. Steele, W. Srituravanich, Y. Pikus, C. Sun, and X. Zhang, "Focusing surface plasmons with a plasmonic lens," Nano. Lett. **5**, 1726-1729 (2005).
18. L. L. Yin, V. K. Vlasko-Vlasov, J. Pearson, J. M. Hiller, J. Hua, U. Welp, D. E. Brown, and C. W. Kimball, "Subwavelength focusing and guiding of surface plasmons," Nano. Lett. 5, 1399-1402 (2005).
19. A. Drezet, A. L. Stepanov, H. Ditlbacher, A. Hohenau, B. Steinberger, F. R. Aussenegg, A. Leitner, and J. R. Krenn, "Surface plasmon propagation in an elliptical corral," Appl. Phys. Lett. **86**, 074104 (2005).
20. Z. W. Liu, J. M. Steele, H. Lee, and X. Zhang, "Tuning the focus of a plasmonic lens by the incident angle," In press Appl. Phys. Lett (2006).
21. H. Raether, *Surface Plasmons on Smooth and Rough Surfaces and on Gratings*. (Springer-Verlag: Berlin, 1988).
22. H. Ditlbacher, J. R. Krenn, A. Hohenau, A. Leitner, and F. R. Aussenegg, "Efficiency of local light-plasmon coupling," Appl. Phys. Lett. **83**, 3665-3667 (2003).
23. J. C. Weeber, M. U. Gonzalez, A. L. Baudrion, and A. Dereux, "Surface plasmon routing along right angle bent metal strips," Appl. Phys. Lett. **87**, 221101 (2005).
24. J. C. Weeber, Y. Lacroute, A. Dereux, E. Devaux, T. Ebbesen, C. Girard, M. U. Gonzalez, and A. L. Baudrion, "Near-field characterization of Bragg mirrors engraved in surface plasmon waveguides," Phys. Rev. B **70**, 235406 (2004).
25. S. H. Chang, S. K. Gray, and G. C. Schatz, "Surface plasmon generation and light transmission by isolated nanoholes and arrays of nanoholes in thin metal films," Opt. Express **13**, 3150-3165 (2005).
26. J. Seidel, S. Grafstrom, L. Eng, and L. Bischoff, "Surface plasmon transmission across narrow grooves in thin silver films," Appl. Phys. Lett. **82**, 1368-1370 (2003).
27. A. Bouhelier, T. Huser, H. Tamaru, H. J. Guntherodt, D. W. Pohl, F. I. Baida, and D. Van Labeke, "Plasmon optics of structured silver films," Phys. Rev. B **63**, 155404 (2001).
28. Z. W. Liu, Q. H. Wei, and X. Zhang, "Surface plasmon interference nanolithography," Nano. Lett. **5**, 957-961 (2005).
29. P. B. Johnson, and R. W. Christy, "Optical-constants of noble-metals," Phys. Rev. B **6**, 4370-4379 (1972).
30. S. R. Sershen, S. L. Westcott, N. J. Halas, and J. L. West, "Independent optically addressable nanoparticle-polymer optomechanical composites," Appl. Phys. Lett. **80**, 4609-4611 (2002).
31. N. Halas, "Playing with plasmons. Tuning the optical resonant properties of metallic nanoshells," MRS Bulletin **30**, 362-367 (2005).

## 1. Introduction

Surface plasmon polariton (SPP) excitations on metallic films and particles have led to many novel applications such as surface plasmon resonance sensing [1-4], surface enhanced Raman scattering [3, 5-8], and plasmonic optical devices [9-12]. In order to integrate these SPP sensing techniques with lab-on-a-chip technologies or opto-electric applications, the plasmon active substrate must be planar. Recent demonstrations of planar plasmon active substrates include fixating nanoparticles to substrates [13, 14] or by fabricating nanoparticles directly onto substrates such as in nanosphere lithography [15, 16]. Recent experiments have also shown the possibility of focusing SPP excitations on a planar film by guiding SPP waves to the focal point of a circular or elliptical shape [17-19]. Plasmonic lenses (PL) use the sharp edge of a circular slit etched through a metal film to couple free space light to SPP waves, focusing the SPP waves to a region in the lens that is subwavelength in size [17]. Introducing multiple rings to form a circular grating whose period is tuned to the SPP wavelength provides a further enhancement of the intensity at the focal point. This circular grating plasmonic lens is tunable in wavelength providing an engineerable parameter that can be

tailored to specific applications, providing a planar counterpart to tunable, plasmon active nanoparticles.

For circular or elliptical PLs excited by normally incident light, SPP waves will concentrate at the focal points of the lens [17-19]. If the incident light is not perpendicular to the substrate, the focal position will depend on the incident angle [20]. With additional rings, the surface plasmons generated at the outer rings interfere with those generated by the inner rings and may also gain a phase change. The spacing between the rings determines the phase mismatch between the waves generated from the inner and outer rings. By tuning to the SPP wavelength, the periodicity provides momentum matching along the circular grating ensuring resonant SPPs excitation at the foci [21, 22]. The circular grating effectively becomes an active coupling element. Recent experiments have shown that metal gratings with a period meeting the Bragg reflection condition constructively reflect SPP waves launched towards the grating from a separate coupling element, behaving as an efficient Bragg mirror [23, 24]. This dependence on grating period allows for the possibility to have different areas of a metal film tuned as a SPP coupler (PLs) or reflector for different incident wavelengths, allowing for multi-color localized sensing of different molecular species.
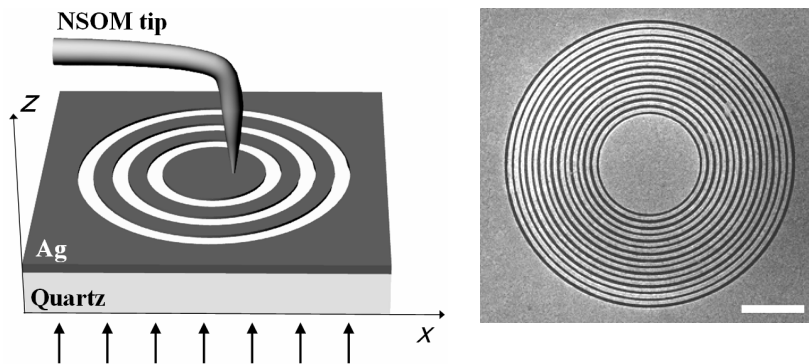


Fig. 1. (a) Experimental scheme for near-field measurements. Circular gratings are cut into a silver film deposited on a quartz substrate. Laser light is normally incident from the quartz side, and the electromagnetic near-field is monitored with a metal coated NSOM tip. (b) SEM image of a sample with 15 rings. The scale bar is 5 microns.

## 2. Experimental method and theoretical modeling

To investigate this concept experimentally, rings with different periods were cut into 150 nm thick silver films. Silver was evaporated onto a quartz plate at a high rate to ensure a surface with minimal roughness. Rings were milled into the metal using an FEI Strata 201 XP focused ion beam (FIB), with the inner most ring having a diameter of 8 microns. Additional rings were added with a period either close to or far from resonance with the excited SPP waves. The surface plasmons were excited with linearly polarized laser light incident from the quartz side. The electromagnetic near-field of these structures was recorded using near-field scanning optical microscopy (NSOM) in collection mode using a metal coated NSOM tip. A metal coated tip was chosen over an uncoated tip to increase the resolution of the scan. Previous experimental results on samples with similar geometry compare favorably with computer simulations, indicating the interaction of the SPP near field with the metal tip is negligible [17, 20]. The measurement scheme can be seen in Fig. 1(a) with an SEM image of a typical sample in Fig. 1(b).

Because the NSOM tip is more sensitive to the components of the near-field parallel to the surface, only those components were calculated [17]. Using polar coordinates as shown in Fig. 2, each point source was centered at a position $\rho_{n,m}(R+mG, \theta_n)$ along the rings, where $R$

is the diameter of the inner circle, $\theta_n$ is the angle from the positive $x$ axis, $G$ is the period of the circular gratings, and $m$ designates in which ring of the grating the point source is located. The electric field of a plasmon point source was quantified by $\dfrac{\cos(\phi)}{\left|\vec{\rho}-\vec{\rho}_{n,m}\right|^{1/2}}$ so that the intensity

has the familiar $\cos^2(\phi)$ and $1/\rho$ dependence [25]. Plasmons were launched perpendicular to the rings, so the angle $\phi$ is measured from $\rho_{n,m}$ as shown in Fig. 2. The polarization of the incident light was chosen to be along the y-axis to match experimental conditions, and to account for this the magnitude of the electric field was multiplied by $sin\,\theta_n$. When SPP waves propagate across a single slit, the transmitted intensity will be modified by the transmission coefficient, T, and the wave will gain a phase, $\Phi$. Crossing multiple gratings is then accounted for by the terms $e^{-im\Phi}$ and $T^m$, where here $m$ signifies the number of gratings crossed while traveling to the center of the pattern. Finally, for simplicity, each ring was modeled to have the same number of point sources. Therefore, to ensure that each ring had the same intensity per unit length, the electric field is multiplied by the factor $(R+mG)/R$. The electromagnetic field of the surface plasmons will then have the following functional form:

$$E_{n,m}^{SPP} = \left[\frac{R+mG}{R}\right]E_0\left|\sin\theta_n\right|T^m e^{-im\Phi}e^{-\left|\vec{\rho}-\vec{\rho}_{n,m}\right|/L_{SPP}}\frac{\cos\phi}{\left|\vec{\rho}-\vec{\rho}_{n,m}\right|^{1/2}}e^{-i\vec{k}_{SP}\bullet(\vec{\rho}-\vec{\rho}_{n,m})} \qquad (1)$$

where the decay length of the surface plasmons, $L_{SPP}$, is also taken into consideration. Note that reflections are not considered in this model as experiments have shown that SPP reflections from subwavelength slits in a metal film are very small [26, 27].
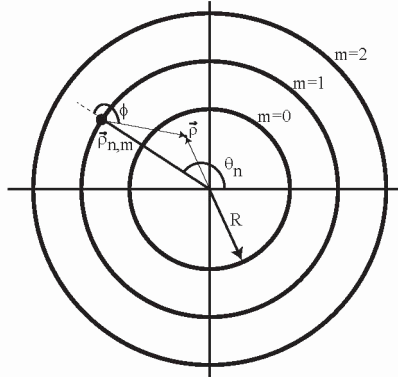


Fig. 2. The near field is modeled as the superposition of the fields from a line of surface plasmon point sources, located at positions $\rho_{n,m}$. $m$ indicates the ring number and $\theta_n$ is the angular position of the point source from the positive x axis. The near field at a point $\rho$ is simply the sum of contributions from all point sources along each ring, $m$. The middle ring is modeled to have a radius of 4 μm with the period of the surrounding ring matching experimental values.

## 3. Experimental results and discussions

Figure 3 shows the cross section of the measured NSOM signal through the center of a sample with four rings along with the calculated intensity from Eq. (1). The figure only shows the inner region of the circle because the transmitted light near the slits overwhelms the near-field signal collected by the NSOM tip. Since the NSOM tip preferentially measures the electric field components parallel to the surface, the near-field shows interference fringes that reach a maximum in the center of the circle [17, 28]. The surface plasmon wavelength and decay length used were 490 nm and 20.4 microns, respectively. These values were

calculated from experimentally obtained dielectric function data for silver for a free-space incident wavelength of 514 nm [29]. The only fitting parameters used for comparing experimental and theoretical values were T, Φ, and a scaling factor. Fitting to the experimental data produced a transmission coefficient of 0.88 and a phase of $0.07\pi$. The high transmission agrees with other experimental studies that launch SPPs across subwavelength slits [26, 27]. The phase change of SPP waves across a barrier is an interesting issue that has received very little attention. If the slit width is much smaller than the SPP wavelength, the slit will have very little effect on the SPP and the phase change should be very small. However, if the slit width is on the order of the SPP wavelength, as the SPP waves cross a slit opposite charges will be induced on opposite sides of the slit, providing quasi-electrostatic coupling across the barrier. Therefore, it is possible that the phase change will be sensitive to the slit width. If the slit width is half the SPP wavelength, the phase change should be zero. The slits milled for these experiments average about 280nm in width, just over half of the SPP wavelength, so a small phase change should be expected. More experimental and theoretical studies are necessary to explore these points.
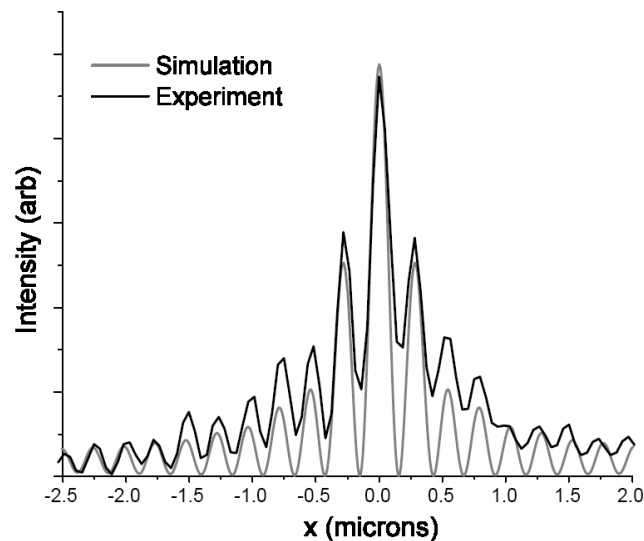


Fig. 3. NSOM measurement of the center region of a sample with 4 rings. The rings have a period of 514 nm, equal to the wavelength of incident light. Similar to the one ring case, the intensity is highest in the center of the circle, indicating that the NSOM tip preferentially measures the in-plane component of the near-field. The theoretical results are also plotted, showing good agreement between experiment and simulation.

Finally, the measured interference period of 242 nm is close to the calculated value of 244 nm or half of the SPP wavelength. This indicates that the interference pattern is solely due to surface plasmons excited on the air side of the silver film interfering with each other and not interfering with any transmitted light [18]. The small difference likely arises from the surface roughness of the silver film causing the surface plasmon wavelength to be different from the calculated value for a smooth surface [21].
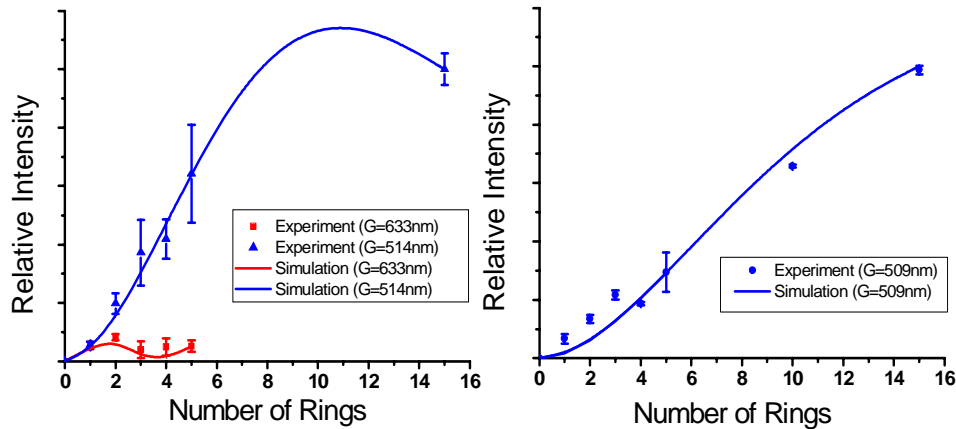
Fig 4. (a) Intensity at the center of the circular grating for increasing number of rings with an incident laser wavelength of 514 nm. Two sets of rings are measured, one with a period G=514 nm and one with G=633 nm. For G=514 nm, the period is close to resonance with the surface plasmon wavelength of 490 nm. The intensity at the center is the result of mostly constructively interfering waves, so the intensity increases with number of rings up to a point, where the intensity levels off. The experimental data matches the simulated data well. For G = 633 nm, the period is off resonance with the surface plasmon wavelength such that each ring as a combination of constructively and destructively interfering waves. (b) Intensity at the center of the circular grating for rings with period G=509 nm exactly resonant with the surface plasmon wavelength for an excitation wavelength of 532 nm. The fitting parameter as defined by Eq. (1) for both figures are: phase=0.07$\pi$, T=0.88. $Lsp$=20.4 $\mu$m in (a) and 25.2 $\mu$m in (b).

Increasing the number of rings generates additional SPP waves that converge to the center of the circle. The period of the rings determines whether the waves will interfere constructively or destructively. Figure 4(a) show the measured intensity at the center of the inner circle as a function of the number of rings for a ring period close to and far from resonance for a silver film with an incident wavelength of 514 nm. Each point represents an average of at least four sets of rings fabricated and measured under identical conditions with the same NSOM tip. Although the laser intensity was kept constant, variations from scan to scan were eliminated by normalizing the intensity at the center of the circles by the maximum intensity recorded by the NSOM tip in the slit region. The calculated intensity at the center of the circle was obtained using Eq. (1), with the same fitting parameters used in Fig. 3 but for different grating periods, *G*. For a period of 633 nm, additional rings do not increase the intensity at the center of the circle, and in some cases decreases the intensity. This is to be expected because the SPP waves are for the most part destructively interfering due to a varying phase mismatch. For a grating period of 514 nm, there will still be a small phase mismatch with a SPP wavelength of 490 nm. This small phase mismatch will increase with each ring added to the PL. If the SPP wave did not decay as it travels along the silver surface, one would expect that the intensity at the center of the PL would oscillate between a minimum and maximum value as additional rings are added. However, because the SPP waves do decay and at each slit a portion of the wave is lost to reflection, the contribution to the intensity at the focal point decreases from each additional ring, damping out the expected oscillations of the focal intensity. In fact, the simulation predicts that the intensity increases at the center of the inner ring up to about 10 rings and then levels off. The experimental results obtained for these conditions match the theoretical results very well.

In principle, if the period of the rings exactly matches the SPP wavelength and the phase gain at each slit is small, additional rings will always increase the intensity of the near-field at the center of the inner ring until the radius of the outermost ring becomes greater than the decay length of the SPP wave. To test this, we fabricated a sample with a 509 nm grating period, which is the theoretical SPP wavelength at the air/silver interface for an incident wavelength of 532 nm. Figure 4(b) presents the experimental results. The intensity at the center of the lens always increases with the number of rings. This increase is likely to continue for samples with more than fifteen rings, provided a small phase mismatch exists between the rings. The experimental results again agree well with the calculated results using Eq. (1). For 15 rings, the intensity at the focus point is an order of magnitude larger than that of a single ring.

In most sensing applications or enhanced Raman scattering, the highest possible near-field intensity is favorable. For circular grating plasmonic lenses, the intensity at the focal point increases with additional resonant rings in the circular grating until the radius of the plasmonic lens reaches the SPP decay length. If non-polarized light is used instead of the linearly polarized light used here, the entire plasmonic lens will generate and focus SPP waves, increasing the near-field intensity at the focal point. The maximum achievable intensity at the focal point ultimately depends in the transmission coefficient T and the SPP decay length $L_{SPP}$ as defined in Eq. (1). Practically, T could be improved by narrowing the grating slit widths, thereby decreasing the barrier encountered by the SPP wave, but $L_{SPP}$ is determined by the desired incident wavelength and film material. However, by tailoring the grating period, slit width, number of slits, and film material, it should be possible to meet the requirements of any application.

There are already many application that use the tunable plasmon resonances of nano-structures to operate in specific regions of the electromagnetic spectrum.[5, 8, 30, 31] The circular grating plasmon lens is a new type of nano-structure amenable to planar architectures. One possible application would be to create different plasmonic lenses tuned to different wavelengths on a single chip. Upon exposure to a certain wavelength of light only plasmonic lenses tuned to the specific SPP wavelength would have an enhanced near-field. The resulting pattern of "hot-spots" would make it possible to monitor different fluorescent molecules and track separate biological processes. Circular grating plasmon lenses therefore combine the flexibility of plasmonic particles with the convenience of a planar structure, allowing for the possibility to easily achieve multi-color sensing on one substrate.

## 4. Conclusions

In conclusion, we have demonstrated the generation and focusing of SPP waves with a planar circular grating based plasmonic lens. The addition of rings to the plasmonic lens increases the intensity at the focal point if the period of the rings is resonant with the SPP wavelength. If the period of the additional rings are not resonant with the SPP wavelength, waves launched towards the center of the lens destructively interfere and there is no intensity increase at the focal point. The number and period of rings, film material, and slit geometries provide experimental handles to tune the plasmonic lens to accommodate specific applications, making this technique a flexible plasmonic tool for sensing applications.

## Acknowledgments